Stopping light using a transient Bragg grating

Tal A. Weiss

Department of Physics, Ben-Gurion University of the Negev, Beer-Sheva 8410501, Israel

Yonatan Sivan [*]

School of Electrical and Computer Engineering, Ben-Gurion University of the Negev, Beer-Sheva 8410501, Israel

We employ a recently developed optical pulse propagation formulation suitable for slow and stopped light regimes to demonstrate light stopping by a (transient) grating coupling in a toy system, which is, however, applicable to a range of wave systems. We study the complete spatiotemporal dynamics, the characteristic timescales, the coupling efficiencies, and the spectral contents of the stopped pulse. Finally, we demonstrate numerically a delay line which surpasses the delay-bandwidth limit.

I. INTRODUCTION

Light has the maximal possible speed. In recent decades, efforts have been made to slow down the speed of light and even to bring it to a complete standstill [1–5]. In addition to being a fundamentally intriguing challenge, slow and stopped light may find practical use for information storage in optical communication systems [6–9], thresholdless lasing [10,11], and quantum optics applications [4,12–17].

Attempts to slow and stop light were based on two generic schemes [5]. First, atomic and molecular media were used for the effective reduction of light speed. Specifically, upon photon absorption, the electromagnetic energy is transferred to electrons excited above their ground state; when the energy is reemitted, the electromagnetic wave seems to propagate at a slower velocity [2,3,18–22]. This approach was overall successful, but its practicality was limited by the narrowness of the atomic resonances [5]. Additional difficulty in this context is the delay-bandwidth limitation that arises from the need to store multiple pulses in a length-limited structure. Specifically, to ensure that the signal does not spill over into the adjacent bit interval, one requires that the broadening due to dispersion should be less than one-half of the bit interval. This leads to a limitation over the bandwidth of the pulse which depends on the group velocity dispersion (GVD) and the length of the structure [5]. These issues can be somewhat mediated using two closely spaced resonances and the concept of electromagnetic-induced transparency. This causes a reduction of the GVD, thus enabling the reduction of the time delay between adjacent pulses [5]. A secondary reason for the delay-bandwidth limitation is the absorption dispersion [5].

The second class of approaches relied on engineering a certain photonic structure such that the dispersion curves characterizing the guided modes propagating in the system include slow light regions and/or a point with a zero group velocity (ZGVP). This occurs, e.g., for arrays of coupled microresonators, photonic crystals, and photonic crystal waveguides (especially near their band edges) [23–25], plasmonic waveguides [10,11,26,27] and negative index metamaterials [28], surface modes in near-zero permittivity metasurfaces [29], etc. One of the advantages of this approach is that high-quality fabrication can reduce the attenuation; the slowdown factors are more modest, but this approach is favorable for high-bit-rate operation [5].

However, having a ZGVP is not enough—one also needs to couple the light to the ZGVP. Unfortunately, it is fundamentally difficult to couple energy to these regimes of slow and stopped light because they are characterized by a very high impedance. Therefore, end-fire excitation schemes suffer from very high reflectivity. This problem can be somewhat mediated by using evanescent wave coupling [30] but overall, poses a severe limitation. Peculiarly, to the best of our knowledge, standard techniques for light coupling such as grating or prism coupling were not applied so far to slow or stopped guided modes. The only exception we are aware of is the numeric study in [31] where a (chirped) grating in a thin metal-dielectric-metal (MDM) waveguide was used to couple light between the propagating symmetric mode and the antisymmetric slow light mode. Unfortunately, in similarity to [32], this study relied on standard coupled mode theory (CMT), which accounts only for the spatial dynamics but neglects temporal dynamics (such as walk off, group velocity dispersion, and higher-order dispersion). Accordingly, the accuracy of that study is limited to the initial stages of the dynamics.

Another suggestion for mediating and/or solving the problem of coupling to the slow or stopped light regime is based on inflection points and degenerate band edges in the dispersion relations of various photonic crystal structures [24]. In these structures, the impedance at the ZGVP is, surprisingly, nonzero. This relatively novel concept has not been demonstrated experimentally, to the best of our knowledge.

Additional recent suggestions to overcome the problem of coupling light to the ZGVP were based on a tapered waveg-

_____

[*]sivanyon@bgu.ac.il

uide [28]. Although initial theory and experimental reports claimed to observe a signature of stopped light [33–35], it was later shown (theoretically, numerically and experimentally) that the incoming pulse is reflected rather than being stopped [36]. Indeed, in [36] it was shown that as the waveguide width narrows, the mode gets closer to the ZGVP such that the coupling to the backward wave (on the other side of the ZGVP) becomes gradually more efficient; eventually, all the energy is coupled to the branch with the backward group velocity rather than being stopped.

In a consequent set of works [10,11,26,37], it was suggested theoretically to circumvent the difficulty associated with the high impedance at the ZGVP by side illumination; in this case, the momentum component of the incoming wave parallel to the interface is identical to the corresponding component of the excited mode. This approach is thus limited to coupling light to the nonguided i.e., radiative modes, those modes that reside above the light line. Thus, by reciprocity, the energy could freely couple back to the free space modes and leak out of the "waveguide." In addition, these suggested implementations relied on high-permittivity components (e.g., semiconductors), which tend to be lossy for the frequency range where the ZGVP points of the studied configuration occurred. Indeed, no experimental verification of this suggestion has been reported so far.

In contrast to the above-mentioned passive attempts to couple light to the slow light regime or to a ZGVP, active approaches were more successful; these studies were sometimes performed in the context of optical nonreciprocity. Specifically, various previous studies attempted to couple light to a slow light or ZGVP by employing transient Bragg grating (TBG) coupling, sometimes referred to as an optical interband transition [38] (both terms essentially equivalent to temporal quasi phase matching [39]). For example, in [40] light coupling to a slow light regime was studied experimentally using a switch pulse which copropagates with the incoming signal pulse. In another set of experiments [41] based on earlier ideas of the Fan group [42,43], effective stopping of light was demonstrated by coupling an optical pulse propagating in a waveguide to a cavity (a ring resonator) and then adiabatically perturbing the system to prevent further coupling back to the waveguide. This allows light to be stored in the cavity for arbitrarily long times; it could be then released at will by turning off the perturbation. The procedure resulted in some spectral modification of the output pulse with respect to the input one associated with the long recombination time of the free-carrier-generation–based perturbation. This active tuning approach exhibits nearly 50% efficiency and overcomes the traditional delay-bandwidth limitation.

While the scheme of [41–43] is effective and can be integrated with existing optical systems, it does not involve true light stopping but instead, pulse storage in a cavity (i.e., the light speed remains high). Furthermore, being experimental in nature, it did not reveal the complete parametric dependence on the group velocity or GVD etc., which is necessary for optimization of the conversion efficiency.

In this article, we show theoretically how light can be truly stopped by coupling a propagating mode to the ZGVP or slow light regime in a waveguide by combining the standard (yet untested, in the current context) approach of grating coupling

with an active approach. The formulation we use is an extension of the momentum-based expansion introduced in [44] to the study of multiple mode coupling. In Sec. II, we describe a toy physical configuration (a grating in a MDM waveguide, as in [31]) and derive the underlying propagation equations for the pulse envelopes, including in the presence of absorption. Unlike the previous works quoted above, we provide a complete quantitative analysis of the spatiotemporal dynamics for horizontal [45,46], vertical [47–51], and oblique transitions between modes across the dispersion curves. Specifically, in Sec. III, we provide a heuristic analysis, and in Sec. IV, we employ numerical simulations to demonstrate pulse stopping and release by coupling energy to the ZGVP. When possible, we complement the numerical simulations with analytic solutions that reveal the parametric dependence on the group velocity mismatch etc. This shows that the conversion efficiency is essentially limited by walk off. In Sec. V we discuss implementation and possible follow-up works.

II. METHODOLOGY AND CONFIGURATION

To date, most theoretical studies of pulse dynamics in the slow and stopped light regimes have been performed with finite difference time domain (FDTD) simulations [52], an approach which is accurate but computationally heavy [11,26]; this approach also does not readily provide analytic insights regarding the underlying physics and parametric dependence. The computationally lighter envelope formulations and associated coupled-mode analysis are unsuitable to this configuration because the standard frequency-based dispersion expansion coefficients diverge near the ZGVP [44]; this makes the truncation of the dispersion expansion inaccurate and its inclusion inefficient.

In [44] we showed that this problem can be circumvented by expanding the dispersion in a series of *spatial* derivatives rather than *temporal* derivatives, such that the divergence of the coefficients is avoided, and instead, rapid convergence is obtained. We solved the resulting equation as an initial value problem in time by constructing the input pulse in momentum space (i.e., as a superposition of plane waves with different momenta). This approach also provides a natural way to treat wave attenuation in waveguides made of absorbing materials which appear in the complex modal frequency.

Here, in analogy to the recent derivation of coupled-mode theory for pulse propagation in time-varying media [53–55], we extend the momentum-based expansion of [44] for the pulse propagation scheme for the slow and stopped light regimes to allow accounting for mode coupling due to a spatiotemporal perturbation of the dielectric constant. Specifically, we consider a situation in which a pulse which initially belongs to a branch with a "regular group" velocity (denoted with index 1) is coupled to the ZGVP (index 2) using a suitable perturbation, specifically, a spatiotemporal grating (aka as a transient Bragg grating, TBG), see Fig. 1(a). In this case, the total field is given by

$$\vec{E}(\vec{r}_\perp, z, t) = \mathcal{F}_\beta^z [\tilde{a}_1(\beta - \beta_{0,1}, t)\tilde{\vec{e}}_1(\vec{r}_\perp, \beta)e^{-i\omega_1(\beta)t}$$
$$+ \tilde{a}_2(\beta - \beta_{0,2}, t)\tilde{\vec{e}}_2(\vec{r}_\perp, \beta)e^{-i\omega_2(\beta)t}], \quad (1)$$
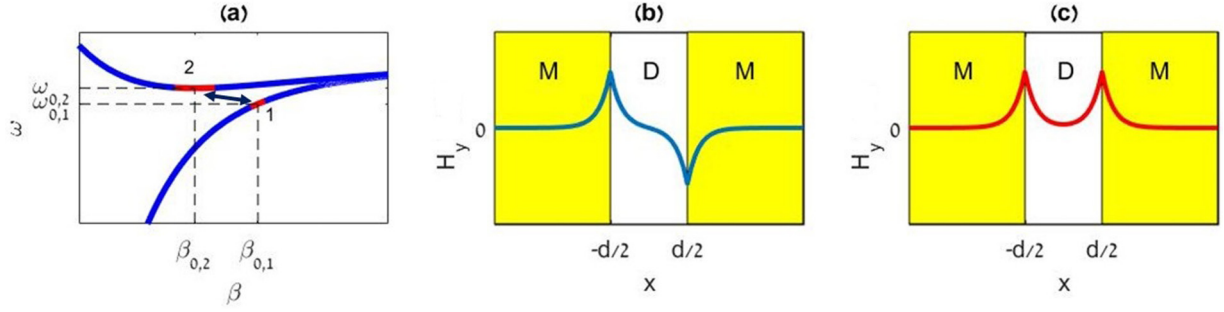
FIG. 1. (a) Schematic dispersion curve of the symmetric and antisymmetric branches of the MDM waveguide. The numbers correspond to the symmetric branch (1) and the antisymmetric branch (2). The red regimes demonstrate spectral regimes centered at $(\beta_{0,1}, \omega_{0,1})$ and $(\beta_{0,2}, \omega_{0,2})$, corresponding to the signal pulse and the stopped pulse, respectively. The arrows demonstrate the flow of energy from the symmetric branch to the ZGVP modes and vice versa due to spatiotemporal perturbation with frequency $\tilde{\omega} = \omega_{0,2} - \omega_{0,1}$ and wave number $\tilde{\beta} = \beta_{0,2} - \beta_{0,1}$. (b) and (c) correspond to schematic modes of the antisymmetric and the symmetric branches, respectively, of a MDM waveguide of width d.

where $\mathcal{F}_{\beta}^{z} \equiv \int_{-\infty}^{\infty} e^{i\beta z} d\beta$, ω_j is the frequency of the monochromatic waves constituting pulse j, and $\tilde{a}_j$ represents the slowly varying amplitudes of a wave packet composed of waveguide modes with different wave numbers centered at the different central momenta $\beta_{0,j}$; $\tilde{\tilde{e}}_j(\vec{r}_\perp, \beta)$ satisfies the vector Helmholtz equation

$$\nabla \times \nabla \times \tilde{\tilde{e}}_j(\vec{r}_\perp, \beta) - \mu\epsilon(\vec{r}_\perp, z, \omega_j(\beta))\omega^2\tilde{\tilde{e}}_j = 0. \quad (2)$$

Here, the modal frequency and permittivity are assumed to be a function of the (modal) momentum β. In lossy media, the resulting modal frequency is complex and can be described only using analytic formulas or by using auxiliary equations for the polarization [52] (rather than experimentally measured tabulated data for the permittivity), which are limited to real frequencies. This limitation is typical to the use of quasinormal modes, see discussions in, e.g., [56,57].

For concreteness, we assume that the two pulses belong to different branches (i.e., we study the so-called "interband" transition [38,39]) of different symmetries,[1] see Figs. 1(b) and 1(c), such that they are coupled by any (transversely) asymmetric perturbation; this is the case for a simple thin MDM slab waveguide with a symmetric cladding, see [44] and references therein. Specifically, the permittivity perturbation is assumed to be a TBG, namely, to have the form

$$\Delta\tilde{\epsilon}(\vec{r}_\perp, z, t) = \overline{\Delta\epsilon}W(\vec{r}_\perp)q(z)m(t)\cos(\tilde{\omega}t)\cos(\tilde{\beta}z), \quad (3)$$

where $\overline{\Delta\epsilon}$ is the dimensionless magnitude of the permittivity perturbation, $m(t)$, $W(\vec{r}_\perp)$, and $q(z)$ are unity-amplitude (i.e., $\max[m(t)] = 1$, $\max[W(\vec{r}_\perp)] = 1$ and $\max[q(z)] = 1$), dimensionless functions representing the temporal and (transverse and longitudinal) spatial "slowly varying envelopes" of the perturbation, respectively; for concreteness, $W(\vec{r}_\perp)$ is assumed asymmetric. $\tilde{\omega}$ and $\tilde{\beta}$ represent the central temporal and spatial frequencies of the perturbation, i.e., the rapidly oscillating components of the TBG, which provide the missing spatial (and temporal) frequencies to bridge the mode mismatch, thus enabling an efficient coupling. For convenience,

we chose $\tilde{\omega} \equiv \omega_{0,2} - \omega_{0,1}$ and $\tilde{\beta} \equiv \beta_{0,2} - \beta_{0,1}$ to match the relevant (generally oblique) transition, see Fig. 1(a).

In this case, the coupled-mode theory equations for the amplitudes of the two pulses are given, up to second-order (i.e., group velocity) dispersion, by

$$\frac{\partial A_1(z,t)}{\partial t} + v_{g,1}\frac{\partial A_1(z,t)}{\partial z} - i\frac{\omega_{0,1}''}{2}\frac{\partial^2 A_1(z,t)}{\partial z^2} - i\omega_{0,1}\overline{\Delta\epsilon}|\mathcal{O}|e^{i\delta}m(t)A_2(z,t) = 0, \quad (4)$$

$$\frac{\partial A_2(z,t)}{\partial t} - i\frac{\omega_{0,2}''}{2}\frac{\partial^2 A_2(z,t)}{\partial z^2} - i\omega_{0,2}\overline{\Delta\epsilon}|\mathcal{O}|e^{-i\delta}m(t)A_1(z,t) = 0, \quad (5)$$

see derivation in [58] and in Appendix A. Here, A_j are the slowly varying amplitudes of the two different pulses, defined via

$$A_j(z,t) = 2\pi e^{-i\beta_{0,j}z}\mathcal{F}_{\beta}^{z}[\tilde{a}_j(\beta - \beta_{0,j}, t)e^{-i[\omega_j(\beta) - \omega_{0,j}]t}], \quad (6)$$

where $\omega_{0,j} = \omega(\beta_{0,j})$, $v_{g,j}$, and $\omega_{0,j}''$ are their central frequencies, group velocities, and group velocity dispersion (GVD) coefficients, respectively. Furthermore, $\mathcal{O}_{ij}$ is the dimensionless coupling coefficient given by

$$\mathcal{O}_{j,j'}(\beta, \beta_{0,j}) = \epsilon_0\frac{\int W(\vec{r}_\perp)\tilde{\tilde{e}}_j(\vec{r}_\perp, \beta)\tilde{\tilde{e}}_{j'}^*(\vec{r}_\perp, \beta)d\vec{r}_\perp}{U_{j,j'}(\beta, \beta_{0,j})}, \quad (7)$$

where we normalize by the (potentially complex) quantity

$$U_{j,j'}(\beta, \beta_{0,j}) = \int \left(\epsilon(\vec{r}_\perp, \omega) + \frac{\omega}{2}\frac{\epsilon(\vec{r}_\perp, \omega)}{d\omega}\right)\Bigg|_{\omega_{0,j}}$$
$$\times \tilde{\tilde{e}}_j(\vec{r}_\perp, \beta)\tilde{\tilde{e}}_{j'}^*(\vec{r}_\perp, \beta)d\vec{r}_\perp. \quad (8)$$

As shown in [44], in the case of lossless media, $U_{j,j}(\beta_{0,j}, \beta_{0,j})$ is a real quantity proportional to the energy density (per unit length) of the carrier mode $\beta_{0,j}$ of pulse j.[2] In the current context of two modes of different symmetries, $U_{j,j'}$ is diagonal, see Appendix A. Lastly, $\delta = \arg(\mathcal{O}_{1,2}) = -\arg(\mathcal{O}_{2,1})$ is the

---

[1]In this case, if $\epsilon(\vec{r}_\perp, \omega)$ is symmetric in $\vec{r}_\perp$, the two modes are decoupled in the absence of a perturbation.

[2]Note that this statement refines the slightly inaccurate explanation in [44].

phase of the coupling coefficient. Since $\overline{\Delta\epsilon}$ and $|\mathcal{O}_{i,j}|$ appear together, it is convenient to refer to them as a single parameter; for simplicity, we just set $|\mathcal{O}_{i,j}| = 1$.

The temporal profile of the perturbation is assumed to be

$$m(t) = e^{-[(t-t_m)/T_{sw}]^2}, \tag{9}$$

where the switching time, T_{sw}, represents the duration of the perturbation, and t_m (chosen for convenience such that it is much longer than T_{sw}) represents the time at which the perturbation peaks. For simplicity, we assumed below $q(z) = 1$.

Following [44], Eqs. (4) and (5) are solved as an initial value problem in time. Specifically, the initial condition for this set of equations is written in momentum space, $\tilde{a}_1(\beta - \beta_{0,1}, t = 0) = \frac{\sqrt{\pi}}{Z} e^{(\frac{\beta-\beta_{0,1}}{2Z^{-1}})^2}$, where $Z = \frac{2}{\Delta\beta}$ is the initial spatial length of the input pulse. Thus, in real space, the initial envelope profile is

$$A_1(z, t = 0) = e^{-(\frac{z}{Z})^2}. \tag{10}$$

The initial pulse of the stopped light has zero amplitude, namely, $A_2(z, t = 0) = 0$.

III. HEURISTIC ANALYSIS

The dynamics of the two interacting pulses, represented by the solution of Eqs. (4) and (5), can be characterized by the interplay between the duration of the perturbation (i.e., the switching time, T_{sw}) and two additional timescales. First, the timescale representing the propagation of the input signal pulse can be defined as $T_w \equiv Z/|v_{g,1} - v_{g,2}| = Z/v_{g,1}$ (since $v_{g,2}$ corresponds to the stopped light branch); this timescale is nothing but the standard walk-off scale (see, e.g., [59])—it describes the time required for the signal pulse to propagate a distance comparable to its own initial spatial extent [relative to the (stopped) pulse it interacts with]. In the current context, in which one pulse is static, this timescale is essentially the incident pulse duration such that it can naturally be tuned via that initial extent. Second, the timescale that represents the rate of energy exchange between the pulses is given (in the absence of any walk off) by the (generalized) Rabi period $T_R \equiv 2\pi(\sqrt{\omega_{0,1}\omega_{0,2}}\overline{\Delta\epsilon})^{-1}$, see derivation in Appendix B. Notably, the definition of T_R here adds upon the analysis performed in some of our previous work (specifically, [50,51,60]).

These timescales allow us to interpret the dynamics in two limits—if the switching time T_{sw} is much shorter than the walk-off time T_w, the pulses are essentially static during their mutual interaction so that the energy exchange between the pulses occurs under conditions of a good (and time-invariant) spatial overlap. This case is similar to the standard two-level system [61] in the sense that it lacks spatial dynamics; hence, the exchange is relatively efficient and complete energy exchange can be achieved if $T_{sw} \sim T_R/2 \ll T_w$. In that sense, this interaction is nonadiabatic [46,50,51] such that the shape and spectrum of the stopped pulse are similar to those of the incident pulse. This behavior has a simple interpretation. As explained in [46,50,51], the short perturbation is also broad spectrally with respect to $1/T_w$ such that all the frequency components in the signal pulse can find the necessary momentum and frequency components needed to phase-match

them to the ZGVP. Therefore, the spectra of the signal pulse is transferred efficiently to the ZGVP branch. As the perturbation becomes longer in time, it narrows in spectrum such that less frequency components of the signal pulse are phase matched. The resulting stopped pulse is spectrally narrower. In this way, by controlling the switching time, one can filter the spectrum of the stored pulse.

If, on the other hand, the walk-off time is comparable to or even shorter than the (generalized) Rabi period, then the spatial overlap between the two pulses deteriorates during the switching time so that the energy exchange becomes slower and spreads over a wider portion of space. As a result, different regions of space might exhibit different rates of energy exchange, the overall dynamics is more complicated, the stopped pulse becomes smeared in space and only a partial transfer of energy to the ZGVP can be achieved (with an overall decrease of the coupling efficiency for faster walk off).

IV. RESULTS

We now demonstrate the validity of the intuitive picture via numerical simulations. All numerical simulations below are performed for $\beta_{0,1} = 2 \times 10^8$ m^{-1}, $\beta_{0,2} = 1.5 \times 10^8$ m^{-1}, and $\omega_{0,1} = \omega_{0,2} = 5.184 \times 10^{15}$ s^{-1} (i.e., a horizontal transition over the energy-momentum dispersion relation), which results in $v_{g,1} = 1.3 \times 10^{-3}$ c. The initial condition corresponds to $\Delta\beta = 10^7$ m^{-1} so that $Z = 0.2$ μm and $T_w = 0.52$ ps. The duration of the simulations below is significantly shorter than the dispersion time [44], so that the GVD-induced broadening is weak. In order to focus on the coupling dynamics, we neglect below the absorption loss in the metal.

A. Numerical results – Stopping light

Figure 2 shows the numerical solution of Eqs. (4) and (5) for negligible walk off ($T_{sw} \ll T_w$). The incoming signal pulse propagates at a velocity $v_{g,1}$ and undergoes very weak dispersive broadening during the simulation time, see Figs. 2(a) and 2(b). The pulse that is coupled to the ZGVP builds up at around t_m and indeed remains static; it also undergoes only weak dispersive broadening. As expected, the most efficient coupling occurs when the switching time is half of the Rabi period [Figs. 2(d)–2(e)], and the least efficient conversion occurs when it is chosen to be a full Rabi period [Figs. 2(g) and 2(h)].

Figures 3(a) and 3(b) show the corresponding numerical results for $T_{sw} \gg T_w$. In this case, the more significant walk off results in more complicated dynamics. Specifically, as the signal pulse now propagates relatively faster with respect to the energy exchange rate ($T_w/T_R = 1/16$), it effectively transfers its energy to the stopped pulse over an extended segment of space at roughly the same efficiency, causing the stopped pulse to smear out in space; this causes the energy transfer to the stopped pulse to be lower overall and to continue beyond $t = T_R/2$. Furthermore, one can see energy transfer back to the signal branch.

In that sense, not only does the stopped pulse become distorted with respect to the incoming signal pulse, but also the signal pulse develops additional lobes in its trailing edge. This effect is accompanied by the signal depletion.
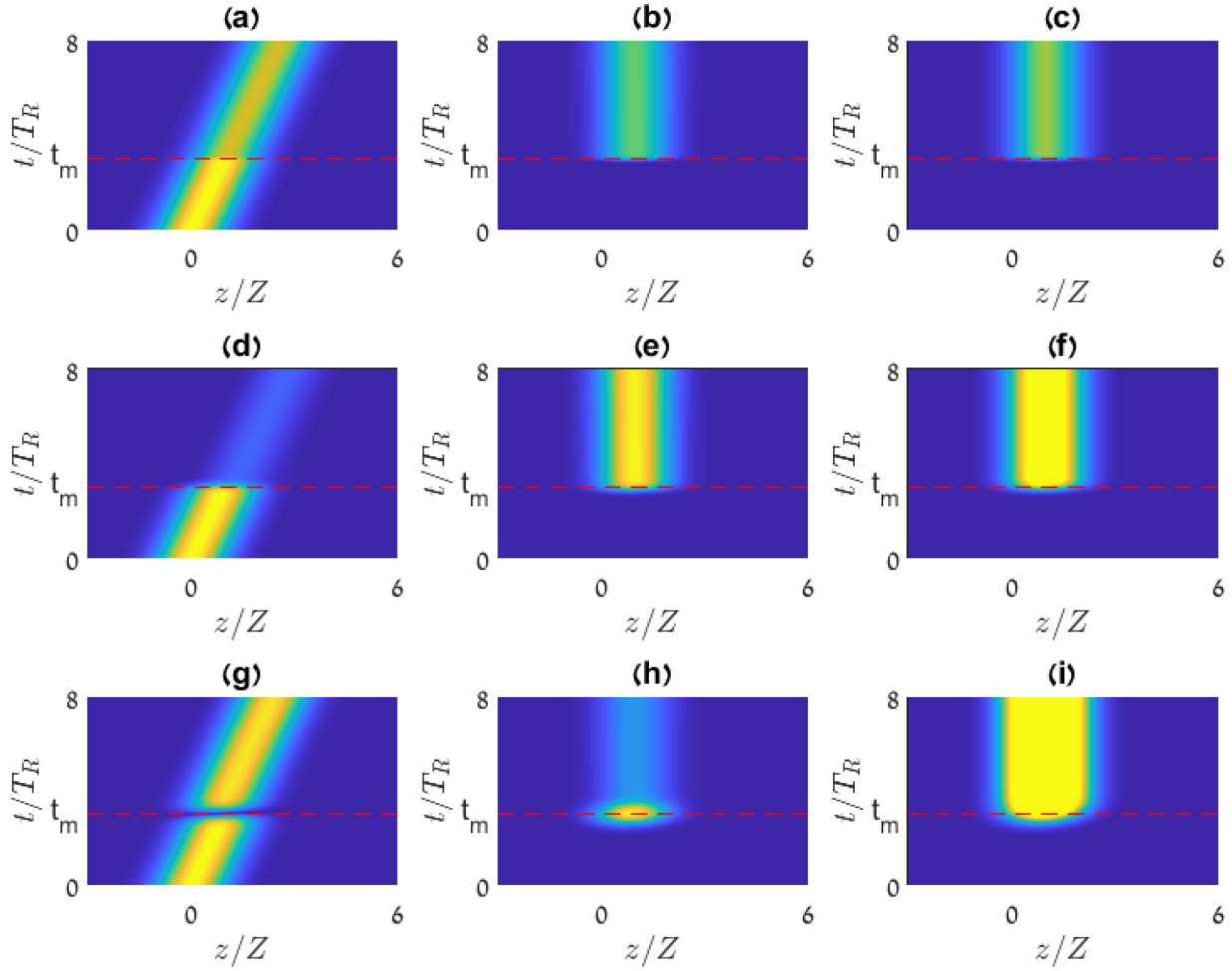
FIG. 2. Maps of the spatiotemporal dynamics of the signal [(a), (d), and (g); solutions of Eq. (4)] and the corresponding stopped pulses [all other subplots; solutions of Eq. (5)] with the perturbation parameters of the form (9) and the spectral parameters indicated in the main text. The magnitude of the perturbation is $\overline{\Delta\epsilon} = 3.6 \times 10^{-3}$, which results in $T_R = 0.3T_w$. The total duration of propagation of all pulses presented is $8T_R = 1.3$ ps. In all cases, $t_m = 3T_R$, where the switching times are (a)–(c) $T_{sw} = 0.25T_R$, (d)–(f) $T_{sw} = 0.5T_R$, and (g)–(i) $T_{sw} = T_R$. (c), (f), and (i) show the analytic solution (11) for each row. In all color maps, the amplitudes vary in the range [0, 1].

In Figs. 4(a) and 4(b) we now show the spectrum of the stopped pulse in momentum space, long after the permittivity perturbation vanished. For simplicity, we set $T_R \gg T_w$. In the nonadiabatic limit [$T_{sw} \ll T_w$, Fig. 4(a); nonadiabatic limit], the spectrum of the stopped pulse is nearly identical to the spectrum of the incoming pulse, while away from that limit

[Fig. 4(b)], the spectrum of the stopped pulse is narrower. This result is similar to those obtained in previous studies of nonadiabatic pulse interactions, e.g., for the case of wavefront reversal due to the coupling of pulses with opposite momenta [46]. This behavior is in accordance with the analysis presented in Sec. III.
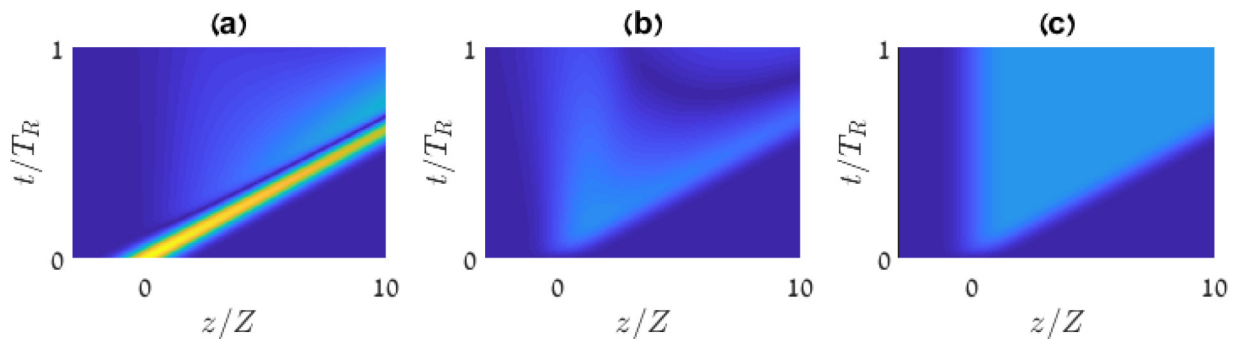

FIG. 3. Dynamics of the (a) signal and the (b) stopped pulse for $\overline{\Delta\epsilon} = 7.2 \times 10^{-5}$ and $T_{sw} \gg T_R = 16T_w$ (other parameters are specified in the main text). (c) The analytic solution (12) corresponding to the stopped pulse. In all color maps, the amplitudes vary in the range [0, 1].
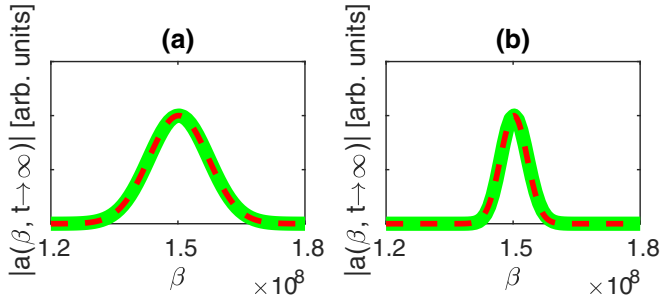
FIG. 4. The spatial spectrum of the stopped pulse as $t \to \infty$ in the case of $T_R = 17$ ps, $T_w = 0.5$ ps and (a) $T_{sw} = 2$ ps and (b) $T_{sw} = 0.1$ ps. In both cases, the green line represents the outcome of the simulation, and the dashed red line corresponds to the analytic solution (12). The corresponding final widths of the spectra are (a) $\Delta \widetilde{\beta} = 10^7$ m^{-1} (as in Figs. 2 and 3; essentially identical to the input spectral width) and (b) $\Delta \widetilde{\beta} = 4.5 \times 10^6$ m^{-1}.

B. Analysis

As long as only a small fraction of the incoming pulse power is coupled to the ZGVP, one can adopt the so-called "undepleted signal approximation" [46,50,51,55,60], namely, to neglect the energy coupling to the stopped pulse such that the signal undergoes unperturbed (dispersive) propagation. In this case, the equation for the dynamics of the stopped pulse can be solved analytically, thus providing a clear picture of the parametric dependence. If one neglects the GVD, this solution is

$$A_2(z,t) = \frac{\sqrt{\pi} T_{sw} Z \omega_{0,2} \overline{\Delta \epsilon}}{\widetilde{Z}} e^{-\frac{(z - v_{g,1} t_m)^2}{\widetilde{Z}^2}}$$
$$\times \left[\text{erf} \left(\frac{\widetilde{Z}}{Z} \frac{t}{T_{sw}} - \frac{T_{sw}}{T_w} \frac{z}{\widetilde{Z}} - \frac{t_m Z}{T_{sw} \widetilde{Z}} \right) \right.$$
$$\left. - \text{erf} \left(-\frac{T_{sw}}{T_w} \frac{z}{\widetilde{Z}} - \frac{t_m Z}{T_{sw} \widetilde{Z}} \right) \right], \quad (11)$$

where $\widetilde{Z}^2 = Z^2 + v_{g,1}^2 T_{sw}^2$. It is insightful to explore Eq. (11) in the limit of $t \to \infty$, i.e., after the perturbation ends (recall that $t_m \gg T_{sw}$).[3] Then, in the nonadiabatic case ($T_{sw} \ll T_w$), Eq. (11) reduces to

$$A_2(z, t \to \infty) = \frac{\sqrt{\pi} T_{sw} Z \omega_{0,2} \overline{\Delta \epsilon}}{\widetilde{Z}} e^{-\frac{(z - v_{g,1} t_m)^2}{\widetilde{Z}^2}}. \quad (12)$$

Thus, the stopped pulse is static and identical in shape to the incoming pulse, as expected.

The analytic solution (11) corresponding to the numeric results is shown in Figs. 2(c), 2(f) and 2(h). In Fig. 2(c), the analytic result matches the numerics reasonably well. Here, the time duration of the energy transfer T_{sw} is short enough with respect to T_R to permit the undepleted signal approximation. In Fig. 2(f), T_{sw} is longer, and therefore more energy is transferred to the stopped pulse. In this case, the undepleted signal approximation breaks down such that the analytic result matches the numeric one qualitatively but not

---

[3] Note that t_m affects only the position of the pulse center. This is seen explicitly in Eq. (12).
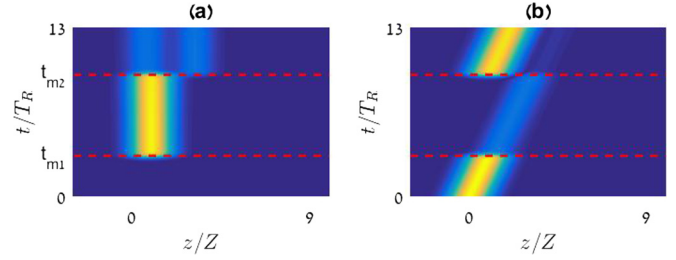

FIG. 5. (a) Stopped and (b) signal pulse dynamics [solutions of Eqs. (4) and (5)] where the perturbation is switched twice (at $t_{m1} = 0.5$ ps and at $t_{m2} = 1.5$ ps). All other parameters are the same as in Fig. 2. In all color maps, the amplitudes vary in the range [0, 1].

quantitatively. In Fig. 2(h), T_{sw} exceeds the time in which the undepleted approximation is valid, and therefore, the analytic solution does not predict the correct ZGVP pulse dynamics in this case even qualitatively.

In order to find an analytic expression for the spectrum dynamics in the stopped light regime at time $t \to \infty$, we apply a spatial Fourier transform to Eq. (12) and get $\mathcal{F}_z^\beta [A_2(z, t \to \infty)] \sim e^{-\left(\frac{\beta}{\Delta \widetilde{\beta}} \right)^2}$, where

$$\Delta \widetilde{\beta} = \frac{2}{\sqrt{Z^2 + v_{g,1}^2 T_{sw}^2 / 4}}. \quad (13)$$

Fitting the Fourier transform of Eq. (12) to the numerical results in Fig. 4 yields an excellent match.

C. Numerical simulations – Delay line

In Sec. IV A, we showed that light can be stored efficiently when employing a perturbation of time duration $T_{sw} = 0.5 T_R$. Correspondingly, when a second perturbation of the same duration occurs, the light can be coupled back into the original branch and resume the forward propagation. Specifically, this would happen if the perturbation is switched at times t_{m1} and t_{m2} according to

$$m(t) = e^{-[(t - t_{m1})/T_{sw}]^2} + e^{-[(t - t_{m2})/T_{sw}]^2}. \quad (14)$$

In Figs. 5(a) and 5(b), we show the dynamics of the stopped and signal pulses, respectively. During the first switching pulse, the energy builds up in the stopped light regime, where it is static until t_{m2}; a small amount of energy is left in the original branch; this imperfect coupling is due to the relative movement of the pulses (walk off; equivalently, the deviation from nonadiabaticity). When the perturbation is switched on again at t_{m2}, most of the energy is coupled back to the signal pulse. At time $t > t_{m2}$ we observe two weak remnants of energy in the stopped light branch. The remnant at the trailing edge is, again, a result of imperfect energy transfer back to the original (forward) branch. The remnant at the leading edge is energy that initially remained in the signal branch and then was coupled to the stopped pulse during the second switching event.

Notably, this active switching approach allows us to surpass the delay-bandwidth limitation, as in previous active switching approaches (see, e.g., [41–43]).

V. IMPLEMENTATION AND OUTLOOK

For simplicity, we analyzed so far an idealized nonlossy MDM waveguide at optical frequencies; however, in practice, such a system is expected to be too lossy. More practical (yet, more complicated) lower-loss optical systems where ZGVPs might be found are photonic crystals (e.g., near the band edges [62–65], as for layered media), photonic crystal waveguides, high-index (e.g., silicon) waveguides, near-zero permittivity metasurfaces based on phononic materials (see [29] and references therein), etc.

The necessary periodic illumination patterns can be generated by direct interference, imaging [66], or through a phase mask (see e.g., [67]). For optical frequencies, the TBG can be based on an incoherent nonlinear optical effect which is associated with an intensity-dependent index change [e.g., the Kerr effect [68], free-carrier (FC) generation [69,70], multiphoton absorption, and (consequent) thermal effects [67,71] etc.]. The slowness usually associated with the latter temporally nonlocal effects can be conveniently circumvented in the TBG configuration—the inherent rapid spatial nonuniformity of the periodic perturbation is washed out by FC or heat diffusion on a relatively fast timescale [67,71,72]. For lower frequencies, the TBG can be realized electronically, as e.g., in [47,73]. Oblique transitions (i.e., moving perturbations) can be realized using coherent three- or four-wave mixing, as e.g., in [38]; these are useful for isolation purposes [38,74].

The ideas explored in the current manuscript are not limited to optical waves. Indeed, they can be applied to the terahertz regime (e.g., employing ultrafast modulations of graphene [74,75]), microwave regime, or to other wave systems such as elastic waves, spin waves [47], water waves [76,77], etc.

The current study focused on relatively ultrafast switching of low-intensity picosecond pulses. For shorter pulses, one would need to account for higher-order dispersion terms. The associated coupling terms become quite involved (see [44]) such that intrapulse coupling and broadening induced by group velocity dispersion or higher-order dispersion will cause distortions of stopped pulse with respect to the signal pulse. However, these distortions are not different, in principle, from those experienced by a pulse propagating in a "regular group velocity" branch for the same duration.

An additional degree of freedom that can allow a higher level of control over the stopped pulse spatiotemporal shape is the spatial extent of the TBG, namely, of $q(z)$. Indeed, the configuration studied above can allow, e.g., a TBG with a finite spatial extent given by

$$q(z) = e^{-((z-z_0)/v_g T_{\text{pass}})^2},\qquad(15)$$

with T_{pass} being an additional timescale that represents the time required for a photon to cross the TBG. For $T_{\text{pass}} \to \infty$, the stopped pulse has the same spatial length as the signal. However, as T_{pass} gets shorter, the stopped pulse shrinks in space. Once T_{pass} becomes the shortest timescale, the modulation samples the signal at a single point [60].

APPENDIX A: DERIVATION OF THE COUPLED-MODE EQUATIONS USING THE MOMENTUM-BASED EXPANSION

We start from the vector wave equation

$$\vec{\nabla} \times \vec{\nabla} \times \vec{E}(\vec{r}_\perp, z, t) - \mu_0 \frac{\partial^2}{\partial t^2}[\vec{P}(\vec{r}_\perp, z, t) + \Delta\vec{P}(\vec{r}_\perp, z, t)] = 0,\qquad(A1)$$

where $\vec{P}(\vec{r}_\perp, z, t) = \mathcal{F}_\omega^t\{[\epsilon(\vec{r}_\perp, \omega) - 1]\mathcal{F}_t^\omega[\vec{E}(\vec{r}_\perp, z, t)]\}$, and where $\Delta\vec{P}(\vec{r}_\perp, z, t)$ is a perturbation which can be caused by any alteration of the permittivities of the constituents such as a nonlinearity or a defect.

In analogy to [55], we use the following ansatz for the electric field:

$$\vec{E}(\vec{r}_\perp, z, t) = \mathcal{F}_\beta^z[\tilde{\vec{E}}(\vec{r}_\perp, \beta, t)] = \mathcal{F}_\beta^z\left[\sum_j \tilde{a}_j(\beta - \beta_{0,j}, t)\tilde{\vec{e}}_j(\vec{r}_\perp, \beta)e^{-i\omega_j(\beta)t}\right]$$

$$= e^{-i\omega_{0,j}t}\mathcal{F}_\beta^z\left[\sum_j\left(\int dz' A_j(z', t)e^{-i(\beta - \beta_{0,j})z'}\right)\left(\int dz'' \mathcal{F}_\beta^{z''}[\tilde{\vec{e}}_j(\vec{r}_\perp, \beta)]e^{-i\beta z''}\right)\right]$$

$$= e^{-i\omega_{0,j}t}\sum_j \int d\zeta A_j(z - \zeta, t)e^{i\beta_{0,j}(z-\zeta)}\mathcal{F}_\beta^\zeta[\tilde{\vec{e}}_j(\vec{r}_\perp, \beta)],\qquad(A2)$$

where j is an index corresponding to the different pulses in the waveguide. Here,

$$A_j(z, t) = 2\pi e^{-i\beta_{0,j}z}\mathcal{F}_\beta^z[a_j(\beta - \beta_{0,j}, t)]\qquad(A3)$$

and

$$a_j(\beta - \beta_{0,j}, t) = \tilde{a}_j(\beta - \beta_{0,j}, t)e^{-i[\omega_j(\beta) - \omega_{0,j}]t},\qquad(A4)$$

where $\beta_{0,j}$ is the central propagation constant of pulse j, $\omega_{0,j} = \omega(\beta_{0,j})$, and $\tilde{\vec{e}}_j(\vec{r}_\perp, \beta)$ satisfies the Helmholtz equation,

$$
\left[\left(\frac{\partial^2 \tilde{e}_y}{\partial x \partial y} - \frac{\partial^2 \tilde{e}_x}{\partial y^2} + \beta^2 \tilde{e}_x + i\beta \frac{\partial^2 \tilde{e}_z}{\partial x}\right)\hat{x} + \left(\frac{\partial^2 \tilde{e}_x}{\partial x \partial y} - \frac{\partial^2 \tilde{e}_y}{\partial x^2} + \beta^2 \tilde{e}_y + i\beta \frac{\partial^2 \tilde{e}_z}{\partial y}\right)\hat{y} + \left(i\beta\left[\frac{\partial \tilde{e}_x}{\partial x} + \frac{\partial \tilde{e}_y}{\partial y}\right] - \frac{\partial^2 \tilde{e}_x}{\partial x^2} - \frac{\partial^2 \tilde{e}_y}{\partial y^2}\right)\hat{z}\right]
$$
$$
+ \mu_0 \epsilon(\vec{r}_\perp, \beta)\omega^2 \tilde{\vec{e}}(\vec{r}_\perp, \beta) = 0,
\tag{A5}
$$

independently for every value of j.

We now use the expansion of the permittivity in time domain,

$$
R(\vec{r}_\perp, t) * \vec{E}(\vec{r}_\perp, z, t) = \sum_{n=0}^{\infty} \frac{i^n}{n!} \left.\frac{d^n \epsilon(\vec{r}_\perp, \omega)}{d\omega^n}\right|_{\omega_0} \frac{\partial^n \vec{E}(\vec{r}_\perp, z, t)}{\partial t^n},
\tag{A6}
$$

where we substitute Eqs. (A6) and (A2)–(A4) in Eq. (A1) and transform to momentum space. This gives

$$
\sum_j \left\{ \left[\left(\frac{\partial^2 \tilde{e}_{y,j}}{\partial x \partial y} - \frac{\partial^2 \tilde{e}_{x,j}}{\partial y^2} + \beta^2 e_{x,j} + i\beta \frac{\partial^2 \tilde{e}_{z,j}}{\partial x}\right)\hat{x} + \left(\frac{\partial^2 \tilde{e}_{x,j}}{\partial x \partial y} - \frac{\partial^2 \tilde{e}_{y,j}}{\partial x^2} + \beta^2 \tilde{e}_{y,j} + i\beta \frac{\partial^2 e_{z,j}}{\partial y}\right)\hat{y} \right.\right.
$$
$$
+ \left.\left(i\beta\left[\frac{\partial \tilde{e}_{x,j}}{\partial x} + \frac{\partial \tilde{e}_{y,j}}{\partial y}\right] - \frac{\partial^2 \tilde{e}_{x,j}}{\partial x^2} - \frac{\partial^2 \tilde{e}_{y,j}}{\partial y^2}\right)\hat{z}\right] a_j(\beta - \beta_{0,j}, t) + \mu_0 \omega_{0,j}^2 \epsilon(\vec{r}_\perp, \omega_{0,j})\tilde{\vec{e}}_j(\vec{r}_\perp, \beta) a_j(\beta - \beta_{0,j}, t)
$$
$$
+ i\mu_0 \tilde{\vec{e}}_j(\vec{r}_\perp, \beta)\left(2\omega_{0,j}\epsilon(\vec{r}_\perp, \omega_{0,j}) + \omega_{0,j}^2 \left.\frac{d\epsilon(\vec{r}_\perp, \omega)}{d\omega}\right|_{\omega_{0,j}}\right)\frac{\partial a_j(\beta - \beta_{0,j}, t)}{\partial t} + \mu_0 \tilde{\vec{e}}_j(\vec{r}_\perp, \beta)\sum_{n=2}^{\infty} i^n \left(\frac{1}{(n-2)!}\left.\frac{d^{n-2}\epsilon(\vec{r}_\perp, \omega)}{d\omega^{n-2}}\right|_{\omega_{0,j}}\right.
$$
$$
\left. + \frac{2}{(n-1)!}\omega_{0,j}\left.\frac{d^{n-1}\epsilon(\vec{r}_\perp, \omega)}{d\omega^{n-1}}\right|_{\omega_{0,j}} + \frac{1}{n!}\omega_{0,j}^2 \left.\frac{d^n \epsilon(\vec{r}_\perp, \omega)}{d\omega^n}\right|_{\omega_{0,j}}\right)\frac{\partial^n a_j(\beta - \beta_{0,j}, t)}{\partial t^n}\right\}e^{-i\omega_{0,j}t} + \frac{\partial^2}{\partial t^2}\mathcal{F}_z^\beta[\Delta\vec{P}(\vec{r}_\perp, z, t)] = 0.
\tag{A7}
$$

Substituting Eq. (A5) in Eq. (A7) allows us to replace the first two terms by $\epsilon(\vec{r}_\perp, \omega)\omega^2 a_j(\beta - \beta_{0,j}, t)\tilde{\vec{e}}_j(\vec{r}_\perp, \beta)$. We now get

$$
\sum_j \left\{ \left[\epsilon(\vec{r}_\perp, \omega)\omega^2 - \epsilon(\vec{r}_\perp, \omega_{0,j})\omega_{0,j}^2\right]a_j(\beta - \beta_{0,j}, t)\tilde{\vec{e}}_j(\vec{r}_\perp, \beta) - i\tilde{\vec{e}}_j(\vec{r}_\perp, \beta)\left(2\omega_{0,j}\epsilon(\vec{r}_\perp, \omega) + \omega_{0,j}^2 \left.\frac{d\epsilon(\vec{r}_\perp, \omega)}{d\omega}\right|_{\omega_{0,j}}\right)\right.
$$
$$
\times \frac{\partial a_j(\beta - \beta_{0,j}, t)}{\partial t} - \tilde{\vec{e}}_j(\vec{r}_\perp, \beta)\sum_{n=2}^{\infty} i^n \left(\frac{1}{(n-2)!}\left.\frac{d^{n-2}\epsilon(\vec{r}_\perp, \omega)}{d\omega^{n-2}}\right|_{\omega_{0,j}} + \frac{2}{(n-1)!}\omega_{0,j}\left.\frac{d^{n-1}\epsilon(\vec{r}_\perp, \omega)}{d\omega^{n-1}}\right|_{\omega_{0,j}}\right.
$$
$$
\left.\left. + \frac{1}{n!}\omega_{0,j}^2 \left.\frac{d^n \epsilon(\vec{r}_\perp, \omega)}{d\omega^n}\right|_{\omega_{0,j}}\right)\frac{\partial^n a_j(\beta - \beta_{0,j}, t)}{\partial t^n}\right\}e^{-i\omega_{0,j}t} - \frac{\partial^2}{\partial t^2}\mathcal{F}_z^\beta[\Delta\vec{P}(\vec{r}_\perp, z, t)] = 0.
\tag{A8}
$$

We now multiply Eq. (A8) by $\tilde{\vec{e}}_{j'}^*(\vec{r}_\perp, \beta)$ and integrate over $\vec{r}_\perp$. This gives

$$
\sum_j \left\{ 2\omega_{0,j}U_{j,j'}(\beta, \beta_{0,j})\frac{\partial a_j(\beta - \beta_{0,j}, t)}{\partial t} + i\left[\int \left(\epsilon(\vec{r}_\perp, \omega)\omega^2 - \epsilon(\vec{r}_\perp, \omega_{0,j})\omega_{0,j}^2\right)\tilde{\vec{e}}_j(\vec{r}_\perp, \beta)\tilde{\vec{e}}_{j'}^*(\vec{r}_\perp, \beta)d\vec{r}_\perp\right]a_j(\beta - \beta_{0,j}, t) \right.
$$
$$
+ i\sum_{n=2}^{\infty} i^n \left[\int \left(\frac{1}{(n-2)!}\left.\frac{d^{n-2}\epsilon(\vec{r}_\perp, \omega)}{d\omega^{n-2}}\right|_{\omega_{0,j}} + \frac{2}{(n-1)!}\omega_{0,j}\left.\frac{d^{n-1}\epsilon(\vec{r}_\perp, \omega)}{d\omega^{n-1}}\right|_{\omega_{0,j}}\right.\right.
$$
$$
\left.\left.+ \frac{1}{n!}\omega_{0,j}^2 \left.\frac{d^n \epsilon(\vec{r}_\perp, \omega)}{d\omega^n}\right|_{\omega_{0,j}}\right)\tilde{\vec{e}}_j(\vec{r}_\perp, \beta)\tilde{\vec{e}}_{j'}^*(\vec{r}_\perp, \beta)d\vec{r}_\perp\right]\frac{\partial^n a_j(\beta - \beta_0, t)}{\partial t^n}\right\}e^{-i\omega_{0,j}t} + i\frac{\partial^2}{\partial t^2}\int \mathcal{F}_z^\beta[\Delta\vec{P}(\vec{r}_\perp, z, t)]\tilde{\vec{e}}_{j'}^*(\vec{r}_\perp, \beta)d\vec{r}_\perp = 0,
\tag{A9}
$$

where we defined

$$
U_{j,j'}(\beta, \beta_{0,j}) = \int \left.\left(\epsilon(\vec{r}_\perp, \omega) + \frac{\omega}{2}\frac{\epsilon(\vec{r}_\perp, \omega)}{d\omega}\right)\right|_{\omega_{0,j}}\tilde{\vec{e}}_j(\vec{r}_\perp, \beta)\tilde{\vec{e}}_{j'}^*(\vec{r}_\perp, \beta)d\vec{r}_\perp.
\tag{A10}
$$

As shown in [44], $U_{j,j}$ is proportional to the energy density of the carrier mode β_0 of pulse j in the case of lossless media.

Equation (A9) represents a set of $\mathcal{N}$ equations, where $\mathcal{N}$ is the number of coupled pulses in the waveguide. Importantly, since $\tilde{\vec{e}}_j$ and $\tilde{\vec{e}}_{j'}^*$ correspond to the same values of β but different values of ω, then they are not orthogonal, so that in general,

$U_{j,j\neq j'}$ is not diagonal ($U_{j,j\neq j'} \neq \delta_{j,j'}$). Accordingly, pulses with a different central frequency are coupled even in the absence of a perturbation (see also [54,56]). We note that the values of $U_{j,j\neq j'}$ may be not negligible with respect to $U_{j,j}$, particularly if j and j' belong to the same branch or for complex systems, where the symmetry is not defined. However, the terms $U_{j,j'\neq j}$ have phase of different frequency, and therefore they are averaged off in time [54].

The system (A9) consists of additional terms of the form

$$\int \frac{d^n \epsilon(\vec{r}_\perp, \omega)}{d\omega^n}\bigg|_{\omega_{0,j}} \tilde{e}_j(\vec{r}_\perp, \beta)\tilde{\bar{e}}_{j'}^*(\vec{r}_\perp, \beta)d\vec{r}_\perp, \tag{A11a}$$

$$\int \frac{d^m \epsilon(\vec{r}_\perp, \omega)}{d\omega^m}\bigg|_{\omega_{0,j}} \tilde{e}_j(\vec{r}_\perp, \beta)\tilde{\bar{e}}_{j'}^*(\vec{r}_\perp, \beta)d\vec{r}_\perp, \tag{A11b}$$

which also contribute to the modal coupling, hence, making the system (A9) even more complicated. These terms do not have an analog in the standard derivation [55], where Eq. (A11a) arises from the expansion of the convolution in Eq. (A6) which is not needed in the standard derivation.

We continue by Taylor expansion of all the functions of ω in terms of β as follows:

$$\sum_j \left\{ 2\omega_{0,j}U_{j,j'}(\beta, \beta_{0,j})\frac{\partial a_j(\beta - \beta_{0,j}, t)}{\partial t} + i\sum_{m=1}^\infty \tilde{D}_m^{j,j'}(\beta - \beta_{0,j})^m a_j(\beta - \beta_{0,j}, t) \right.$$
$$\left. + \sum_{n=2}^\infty \sum_{m=0}^\infty i^{n+1}\tilde{D}_{n,m}^{j,j'}(\beta - \beta_{0,j})^m \frac{\partial^n a_j(\beta - \beta_{0,j}, t)}{\partial t^n} \right\} e^{-i\omega_{0,j}t} + i\frac{\partial^2}{\partial t^2}\int \mathcal{F}_z^\beta[\Delta\vec{P}(\vec{r}_\perp, z, t)]\tilde{\bar{e}}_{j'}^*(\vec{r}_\perp, \beta)d\vec{r}_\perp = 0, \tag{A12}$$

where

$$\tilde{D}_m^{j,j'} = \frac{1}{m!}\frac{d^m}{d\beta^m}\left[\int [\omega^2(\beta)\epsilon(\vec{r}_\perp, \omega(\beta)) - \omega_{0,j}^2\epsilon(\vec{r}_\perp, \omega_{0,j})]\tilde{\bar{e}}_j(\vec{r}_\perp, \beta)\tilde{\bar{e}}_{j'}^*(\vec{r}_\perp, \beta)d\vec{r}_\perp\right]\bigg|_{\beta_{0,j}}, \tag{A13}$$

and

$$\tilde{D}_{n,m}^{j,j'} = \frac{1}{m!}\frac{d^m}{d\beta^m}\left[\int \left(\frac{1}{(n-2)!}\frac{d^{n-2}\epsilon(\vec{r}_\perp, \omega)}{d\omega^{n-2}} + \frac{2}{(n-1)!}\omega_{0,j}\frac{d^{n-1}\epsilon(\vec{r}_\perp, \omega)}{d\omega^{n-1}} + \frac{1}{n!}\omega_{0,j}^2\frac{d^n\epsilon(\vec{r}_\perp, \omega)}{d\omega^n}\right)\tilde{e}_j(\vec{r}_\perp, \beta)\tilde{\bar{e}}_{j'}^*(\vec{r}_\perp, \beta)d\vec{r}_\perp\right]\bigg|_{\omega_{0,j}}. \tag{A14}$$

Transforming Eq. (A12) back to real space, via a shifted Fourier transform ($\mathcal{F}_{\beta-\beta_0}^z$), gives

$$\sum_j \left\{ i\tilde{D}_{2,0}^{j,j'}\frac{\partial^2 A_j(z,t)}{\partial t^2} + \mathcal{F}_{\beta-\beta_0}^z\left[2\omega_{0,j}U_{j,j'}(\beta, \beta_{0,j})\frac{\partial a_j(\beta - \beta_{0,j}, t)}{\partial t}\right] \right.$$

$$+ i\omega_{0,j}'\mathcal{F}_{\beta-\beta_0}^z[2\omega_{0,j}U_{j,j'}(\beta, \beta_{0,j})(\beta - \beta_{0,j})a_j(\beta - \beta_{0,j}, t)] - i\tilde{D}_2^{j,j'}\frac{\partial^2 A_j(z,t)}{\partial z^2}$$

$$\left. + \sum_{m=3}^\infty (-i)^{m-1}\tilde{D}_m^{j,j'}\frac{\partial^m A_j(z,t)}{\partial z^m} + \sum_{n=2}^\infty \sum_{\substack{m=0 \\ m\neq 0 \text{ if } n=2}}^\infty (-1)^m i^{n+m+1}\tilde{D}_{n,m}^{j,j'}\frac{\partial^{n+m}A_j(z,t)}{\partial t^n\partial z^m}\right\} e^{-i\omega_{0,j}t}$$

$$+ i\mathcal{F}_{\beta-\beta_0}^z\left[\frac{\partial^2}{\partial t^2}\int \mathcal{F}_z^\beta[\Delta\vec{P}(\vec{r}_\perp, z, t)]\tilde{\bar{e}}_{j'}^*(\vec{r}_\perp, \beta)d\vec{r}_\perp\right] = 0, \tag{A15}$$

where $\omega_{0,j}' \equiv \frac{d\omega}{d\beta}|_{\beta_{0,j}}$. Equation (A15) represents the full dynamics of the $\mathcal{N}$ pulses propagating in a waveguide.

We apply Eq. (A15) to a symmetric plasmonic slab waveguide as in Fig. 1. Such a structure supports only two modes, a symmetric and an antisymmetric mode. Here, we choose two interacting pulses, corresponding to each branch, namely, $\mathcal{N} = 2$. In this case the electric field is given by

$$\vec{E}(\vec{r}_\perp, z, t) = \vec{E}_1(\vec{r}_\perp, z, t) + \vec{E}_2(\vec{r}_\perp, z, t), \tag{A16}$$

where the indices correspond to the pulse in the antisymmetric and symmetric branches, respectively.

If $\epsilon(\vec{r}_\perp, \omega)$ is symmetric in $\vec{r}_\perp$, the overlap integrals in Eqs. (A10) and (A11) vanish for $j \neq j'$ such that the $\mathcal{N}$ equations in Eq. (A15) are coupled only in the presence of a perturbation, $\Delta\vec{P} \neq 0$.

In the next step, we decompose $\Delta\vec{P}$ as follows:

$$\Delta\vec{P} = \epsilon_0 \Delta\tilde{\epsilon}(\vec{r}_\perp, z, t)\vec{E}(\vec{r}_\perp, z, t), \tag{A17}$$

where $\Delta\tilde{\epsilon}(\vec{r}_\perp, z, t)$ is a dimensionless number which represents the permittivity change. The separation (A17) is valid for temporally and spatially local perturbations (e.g., due to a Kerr media).

Substituting Eq. (A16) and Eq. (A2) in Eq. (A17) gives

$$\Delta\vec{P}(\vec{r}_\perp, z, t) = \epsilon_0 \Delta\tilde{\epsilon}(\vec{r}_\perp, z, t)[A_1(z, t)e^{i(\beta_{0,1}z - \omega_{0,1}t)}\tilde{\vec{e}}_1(\vec{r}_\perp, \beta) + A_2(z, t)e^{i(\beta_{0,2}z - \omega_{0,2}t)}\tilde{\vec{e}}_2(\vec{r}_\perp, \beta)]. \tag{A18}$$

Next, we assume that the perturbation has a separable form, namely,

$$\Delta\tilde{\epsilon}(\vec{r}_\perp, z, t) = \overline{\Delta\epsilon}W(\vec{r}_\perp)q(z)m(t)\cos(\tilde{\omega}t)\cos(\tilde{\beta}z), \tag{A19}$$

where $\overline{\Delta\epsilon}$ is a dimensionless constant carrying the magnitude of the permittivity, $m(t)$ and $q(z)$ are unity-size (i.e., $\max_t[m(t)] = 1$, $\max_z[q(z)] = 1$), dimensionless functions representing the temporal and spatial "slowly varying envelope" of the perturbation, respectively, while $\tilde{\omega}$ and $\tilde{\beta}$ represent the central temporal and spatial frequencies of the perturbation, and $W(\vec{r}_\perp)$ can be any function representing the transverse profile of the perturbation. We further limit ourselves to the case where $W(\vec{r}_\perp)$ is an asymmetric function in $\vec{r}_\perp$. This choice ensures a nonvanishing coupling between the symmetric and antisymmetric modes, as well as a vanishing coupling between modes belonging to the same branch. In this context, it should be noted that while perturbation profiles $W(\vec{r}_\perp)$ with nonantisymmetric profiles would yield a nonvanishing intrabranch coupling, such transitions will typically not be phase matched and hence remain inefficient.

Substituting Eqs. (A17), (A18), and (A19) in Eq. (A15) gives

$$iD_{2,0}^{1,1}\frac{\partial^2 A_1(z,t)}{\partial t^2} + \frac{\partial A_1(z,t)}{\partial t} + v_{g,1}\frac{\partial A_1(z,t)}{\partial z} - i\tilde{D}_2^{1,1}\frac{\partial^2 A_1(z,t)}{\partial z^2} - \frac{iq(z)m(t)e^{i\omega_{0,1}t}}{\omega_{0,1}}$$

$$\times \left\{ \frac{1}{2}[(\omega_{0,1} - \tilde{\omega})^2 e^{-i(\omega_{0,1} - \tilde{\omega})t} + (\omega_{0,1} + \tilde{\omega})^2 e^{-i(\omega_{0,1} + \tilde{\omega})t}]\cos(\tilde{\beta}z)\mathcal{O}_{1,1}A_1(z,t) + \frac{1}{8}[(\omega_{0,2} - \tilde{\omega})^2 e^{-i(\omega_{0,2} - \tilde{\omega})t} \right.$$

$$\left. + (\omega_{0,2} + \tilde{\omega})^2 e^{-i(\omega_{0,2} + \tilde{\omega})t}][e^{i(\beta_{0,2} - \beta_{0,1} + \tilde{\beta})z} + e^{i(\beta_{0,2} - \beta_{0,1} - \tilde{\beta})z}]\mathcal{O}_{1,2}A_2(z,t) \right\} = 0, \tag{A20a}$$

$$iD_{2,0}^{2,2}\frac{\partial^2 A_2(z,t)}{\partial t^2} + \frac{\partial A_2(z,t)}{\partial t} + v_{g,2}\frac{\partial A_2(z,t)}{\partial z} - i\tilde{D}_2^{2,2}\frac{\partial^2 A_2(z,t)}{\partial z^2} - \frac{iq(z)m(t)e^{i\omega_{0,2}t}}{2\omega_{0,2}}$$

$$\times \left\{ [(\omega_{0,1} - \tilde{\omega})^2 e^{-i(\omega_{0,1} - \tilde{\omega})t} + (\omega_{0,1} + \tilde{\omega})^2 e^{-i(\omega_{0,1} + \tilde{\omega})t}]\frac{1}{8}[e^{i(\beta_{0,1} - \beta_{0,2} + \tilde{\beta})z} + e^{i(\beta_{0,1} - \beta_{0,2} - \tilde{\beta})z}]\mathcal{O}_{2,1}A_1(z,t) \right.$$

$$\left. + \frac{1}{2}[(\omega_{0,2} - \tilde{\omega})^2 e^{-i(\omega_{0,2} - \tilde{\omega})t} + (\omega_{0,2} + \tilde{\omega})^2 e^{-i(\omega_{0,2} + \tilde{\omega})t}]\cos(\tilde{\beta}z)\mathcal{O}_{2,2}A_2(z,t) \right\} = 0, \tag{A20b}$$

where we defined $v_{g,1} = \text{Re}(\omega_{0,1}')$, $v_{g,2} = \text{Re}(\omega_{0,2}')$,

$$D_{2,0}^{j,j} = \frac{1}{2\omega_{0,j}U_{j,j'}(\beta, \beta_{0,j})}\tilde{D}_{2,0}^{j,j}, \tag{A21}$$

$$D_2^{j,j} = \frac{\omega_{0,j}''}{2} + D_{2,0}^{j,j}\omega_{0,j}'^2, \tag{A22}$$

and the dimensionless coupling coefficient

$$\mathcal{O}_{j,j'}(\beta) = \epsilon_0 \frac{\int W(\vec{r}_\perp)\tilde{\vec{e}}_j(\vec{r}_\perp, \beta)\tilde{\vec{e}}_{j'}^*(\vec{r}_\perp, \beta)d\vec{r}_\perp}{4U_{j,j'}(\beta, \beta_{0,j})}. \tag{A23}$$

In Eqs. (A20) we omitted the higher-order dispersion terms as their contribution to the pulse propagation is negligible (see [44]). We also omitted terms which are related to absorption such as $\text{Im}[\omega_{0,1}']$. Those terms were found to have a negligible effect on the simulation results (not shown).

We now consider a perturbation where the oscillating terms match the condition $\tilde{\omega} = \omega_{0,2} - \omega_{0,1}$ and $\tilde{\beta} = \beta_{0,2} - \beta_{0,1}$. Equations (A20) then become

$$iD_{2,0}^{1,1}\frac{\partial^2 A_1(z,t)}{\partial t^2} + \frac{\partial A_1(z,t)}{\partial t} + v_{g,1}\frac{\partial A_1(z,t)}{\partial z}$$

$$- i\tilde{D}_2^{1,1}\frac{\partial^2 A_1(z,t)}{\partial z^2} - i\omega_{0,1}q(z)m(t)e^{i\delta}\overline{\Delta\epsilon}|\mathcal{O}|A_2(z,t) = 0, \tag{A24a}$$

$$iD_{2,0}^{2,2}\frac{\partial^2 A_2(z,t)}{\partial t^2} + \frac{\partial A_2(z,t)}{\partial t} + v_{g,2}\frac{\partial A_2(z,t)}{\partial z}$$

$$- i\tilde{D}_2^{2,2}\frac{\partial^2 A_2(z,t)}{\partial z^2} - i\omega_{0,2}q(z)m(t)e^{-i\delta}\overline{\Delta\epsilon}|\mathcal{O}|A_1(z,t) = 0, \tag{A24b}$$

where $|\mathcal{O}| = |\mathcal{O}_{1,2}| = |\mathcal{O}_{2,1}|$ and $\delta = \arg(\mathcal{O}_{1,2}) = -\arg(\mathcal{O}_{2,1})$. In Eqs. (A24) we omitted all the fast oscillating terms as their contribution to the coupling is negligible.

Finally, in order to be able to neglect the nonparaxial terms, we transform both pulses into the reference of the moving frame, and Eq. (A24) then becomes

$$
\frac{\partial A_1(z^*, t^*)}{\partial t^*} - i \frac{\omega''_{0,1}}{2} \frac{\partial^2 A_1(z^*, t^*)}{\partial z^{*2}}
$$
$$
- i\omega_{0,1} q(z^*) m(t^*) e^{i\delta} \overline{\Delta\epsilon} |\mathcal{O}| A_2(z^*, t^*) = 0, \quad \text{(A25a)}
$$

$$
\frac{\partial A_2(z^{**}, t^{**})}{\partial t^{**}} - i \frac{\omega''_{0,2}}{2} \frac{\partial^2 A_2(z^{**}, t^{**})}{\partial z^{**2}} - i\omega_{0,2}
$$
$$
\times q(z^{**}) m(t^{**}) e^{-i\delta} \overline{\Delta\epsilon} |\mathcal{O}| A_1(z^{**}, t^{**}) = 0, \quad \text{(A25b)}
$$

where the new coordinates are

$$
z^* = z - v_{g,1} t, \quad \text{(A26a)}
$$
$$
z^{**} = z - v_{g,2} t, \quad \text{(A26b)}
$$
$$
t^* = t^{**} = t. \quad \text{(A26c)}
$$

Boosting the coordinates back to the laboratory reference, Eqs. (A25) become

$$
\frac{\partial A_1(z, t)}{\partial t} + v_{g,1} \frac{\partial A_1(z, t)}{\partial z} - i \frac{\omega''_{0,1}}{2} \frac{\partial^2 A_1(z, t)}{\partial z^2}
$$
$$
- i\omega_{0,1} q(z) m(t) e^{i\delta} \overline{\Delta\epsilon} |\mathcal{O}| A_2(z, t) = 0, \quad \text{(A27a)}
$$

$$
\frac{\partial A_2(z, t)}{\partial t} + v_{g,2} \frac{\partial A_2(z, t)}{\partial z} - i \frac{\omega''_{0,2}}{2} \frac{\partial^2 A_2(z, t)}{\partial z^2}
$$
$$
- i\omega_{0,2} q(z) m(t) e^{-i\delta} \overline{\Delta\epsilon} |\mathcal{O}| A_1(z, t) = 0. \quad \text{(A27b)}
$$

APPENDIX B: DERIVATION OF THE RABI FREQUENCY

In the case of copropagating pulses, with $v_{g,1} = v_{g,2} = v_g$, we solve Eqs. (A27) in a matrix form as follows:

$$
\left(\frac{\partial}{\partial t} + v_g \frac{\partial}{\partial z} \right) \begin{pmatrix} A_1 \\ A_2 \end{pmatrix} - i\overline{\Delta\epsilon} \begin{pmatrix} 0 & \omega_{0,1} \\ \omega_{0,2} & 0 \end{pmatrix} \begin{pmatrix} A_1 \\ A_2 \end{pmatrix} = 0, \quad \text{(B1)}
$$

where we used the normalization $m = q = 1$ and $|\mathcal{O}| = 1$, and considered a lossless case which results in $\delta = 0$. One of the derivatives can be eliminated by a proper transformation to a moving frame.

Diagonalizing the second matrix in Eq. (B1) gives two eigenvalues, $\pm\sqrt{\omega_{0,1}\omega_{0,2}}\overline{\Delta\epsilon}$, with the corresponding eigenvectors $(\sqrt{\omega_{0,1}}, \pm\sqrt{\omega_{0,2}})/\sqrt{\omega_{0,1}+\omega_{0,2}}$. The solution of Eq. (B1) in the diagonalized basis is then

$$
V_\pm = e^{\pm \frac{i}{2} \sqrt{\omega_{0,1}\omega_{0,2}\overline{\Delta\epsilon}^2}(t - z/v_g)}, \quad \text{(B2)}
$$

where the amplitudes can be found from the eigenvectors setup as follows:

$$
V_\pm = \sqrt{\frac{\omega_{0,1}+\omega_{0,2}}{\omega_{0,2}}} A_1 \pm \sqrt{\frac{\omega_{0,1}+\omega_{0,2}}{\omega_{0,2}}} A_2. \quad \text{(B3)}
$$

Extracting the amplitudes from Eqs. (B2) and (B3) gives

$$
A_1 = \sqrt{\frac{\omega_{0,1}+\omega_{0,2}}{\omega_{0,2}}} \left(\frac{V_+ + V_-}{2} \right)
$$
$$
= \sqrt{\frac{\omega_{0,1}+\omega_{0,2}}{\omega_{0,2}}} \cos\left(\frac{1}{2} \sqrt{\omega_{0,1}\omega_{0,2}}\overline{\Delta\epsilon}(t - z/v_g) \right), \quad \text{(B4a)}
$$

$$
A_2 = \sqrt{\frac{\omega_{0,1}+\omega_{0,2}}{\omega_{0,2}}} \left(\frac{V_+ - V_-}{2} \right)
$$
$$
= \sqrt{\frac{\omega_{0,1}+\omega_{0,2}}{\omega_{0,2}}} i \sin\left(\frac{1}{2} \sqrt{\omega_{0,1}\omega_{0,2}}\overline{\Delta\epsilon}(t - z/v_g) \right). \quad \text{(B4b)}
$$

Equations (B4) represent two propagating pulses, where the energy is perfectly transferred from one pulse to another according to the frequency $\sqrt{\omega_{0,1}\omega_{0,2}}\overline{\Delta\epsilon}$. The oscillations of two coupled states are known as "Rabi oscillations."

[1] D. F. Phillips, A. Fleischhauer, A. Mair, R. L. Walsworth, and M. D. Lukin, Storage of Light in Atomic Vapor, Phys. Rev. Lett. **86**, 783 (2001).

[2] G. Heinze, C. Hubrich, and T. Halfmann, Stopped Light and Image Storage by Electromagnetically Induced Transparency Up to the Regime of One Minute, Phys. Rev. Lett. **111**, 033601 (2013).

[3] R. Won, Quantum memory: Extended storage times, Nat. Photonics **7**, 677 (2013).

[4] G. Brennen, E. Giacobino, and C. Simon, Focus on quantum memory, New J. Phys. **17**, 050201 (2007).

[5] J. B. Khurgin, Slow light in various media: A tutorial, Adv. Opt. Photonics **2**, 287 (2010).

[6] T. Baba, Slow light in photonic crystals, Nat. Photonics **2**, 465 (2008).

[7] T. Tanabe, M. Notomi, E. Kuramochi, A. Shinya, and H. Taniyama, Trapping and delaying photons for one nanosecond in an ultrasmall high-Q photonic-crystal nanocavity, Nat. Photonics **1**, 49 (2007).

[8] M. Notomi, E. Kuramochi, and T. Tanabe, Large-scale arrays of ultrahigh-q coupled nanocavities, Nat. Photonics **2**, 741 (2008).

[9] H. Takesue, N. Matsuda, E. Kuramochi, W. J. Munro, and M. Notomi, An on-chip coupled resonator optical waveguide single-photon buffer, Nat. Commun. **4**, 2725 (2013).

[10] S. Wuestner, T. W. Pickering, J. M. Hamm, A. F. Page, A. Pusch, and O. Hess, Ultrafast dynamics of nanoplasmonic stopped-light lasing, Faraday Discuss. **178**, 307 (2015).

[11] K. L. Tsakmakidis, T. W. Pickering, J. M. Hamm, A. F. Page, and O. Hess, Cavity-free plasmonic nanolasing enabled by dispersionless stopped light, Nat. Commun. **5**, 4972 (2014).

[12] M. Afzelius, N. Gisin, and H. de Riedmatten, Quantum memory for photons, Phys. Today **68**(12), 42 (2015).

[13] H. de Riedmatten, A long-term memory for light, Physics **6**, 80 (2013).

[14] F. Blatt, L. S. Simeonov, T. Halfmann, and T. Peters, Stationary light pulses and narrowband light storage in a laser-cooled ensemble loaded into a hollow-core fiber, Phys. Rev. A **94**, 043833 (2016).

[15] K. V. Rajitha, T. N. Dey, J. Evers, and M. Kiffner, Pulse splitting in light propagation through N-type atomic media due to an interplay of Kerr nonlinearity and group-velocity dispersion, Phys. Rev. A **92**, 023840 (2015).

[16] G. Grigoryan, V. Chaltykyan, E. Gazazyan, O. Tikhova, and V. Paturyan, Pulse propagation, population transfer, and light storage in five-level media, Phys. Rev. A **91**, 023802 (2015).

[17] Y. Chen, Z. Chen, and G. Huang, Storage and retrieval of vector optical solitons via double electromagnetically induced transparency, Phys. Rev. A **91**, 023820 (2015).

[18] M. Fleischhauer, A. Imamoglu, and J. P. Marangos, Electromagnetically induced transparency: Optics in coherent media, Rev. Mod. Phys. **77**, 633 (2005).

[19] P. Siddons, Light propagation through atomic vapours, J. Phys. B: At. Mol. Opt. Phys **47**, 093001 (2014).

[20] L. V. Hau, S. E. Harris, Z. Dutton, and C. H. Behroozi, Light speed reduction to 17 metres per second in an ultracold atomic gas, Nature (London) **397**, 594 (1999).

[21] M. M. Kash, V. A. Sautenkov, A. S. Zibrov, L. Hollberg, G. R. Welch, M. D. Lukin, Y. Rostovtsev, E. S. Fry, and M. O. Scully, Ultraslow Group Velocity and Enhanced Nonlinear Optical Effects in a Coherently Driven Hot Atomic Gas, Phys. Rev. Lett. **82**, 5229 (1999).

[22] P. C. Kuan, C. Huang, W. S. Chan, S. Kosen, and S. Y. Lan, Large Fizeau's light-dragging effect in a moving electromagnetically induced transparent medium, Nat. Commun. **7**, 13030 (2016).

[23] J. D. Joannopoulos, S. G. Johnson, J. N. Winn, and R. D. Meade, *Photonic Crystals - Molding the Flow of Light*, 2nd ed. (Princeton University Press, Princeton, NJ, 2008).

[24] A. Figotin and I. Vitebskiy, Slow light in photonic crystals, Waves Random Complex Media **16**, 293 (2006).

[25] J. E. Sipe, Vector $k \cdot p$ approach for photonic band structures, Phys. Rev. E **62**, 5672 (2000).

[26] K. L. Tsakmakidis, T. W. Pickering, J. M. Hamm, A. F. Page, and O. Hess, Completely Stopped and Dispersionless Light in Plasmonic Waveguides, Phys. Rev. Lett. **112**, 167401 (2014).

[27] M. Reza, M. M. Dignam, and S. Hughes, Can light be stopped in realistic metamaterials? Nature (London) **455**, E10 (2008).

[28] K. L. Tsakmakidis, A. D. Boardman, and O. Hess, 'Trapped rainbow' storage of light in metamaterials, Nature (London) **450**, 397 (2006).

[29] S. Campione, I. Brener, and F. Marquier, Theory of epsilon-near-zero modes in ultrathin films, Phys. Rev. B **91**, 121408(R) (2015).

[30] C. Martijn de Sterke, K. B. Dossou, T. P. White, L. C. Botten, and R. C. McPhedran, Efficient coupling into slow light photonic crystal waveguide without transition region: Role of evanescent modes, Opt. Express **17**, 17338 (2009).

[31] J. Kim, S.-Y. Lee, H. Park, H. Kim, and B. Lee, Slow surface plasmon pulse excitation in metal-insulator-metal plasmonic waveguide with chirped grating, Opt. Express **22**, 18464 (2014).

[32] A. Karenowska, J. Gregg, V. Tiberkevich, A. Slavin, A. Chumak, A. Serga, and B. Hillebrands, Oscillatory Energy Exchange between Waves Coupled by a Dynamic Artificial Crystal, Phys. Rev. Lett. **108**, 015505 (2012).

[33] Q. Gan, Z. Fu, Y. J. Ding, and F. J. Bartoli, Ultrawide-Bandwidth Slow-Light System Based on THz Plasmonic Graded Metallic Grating Structures, Phys. Rev. Lett. **100**, 256803 (2008).

[34] Q. Gan, Y. Gao, K. Wagner, D. Vezenov, Y. J. Ding, and F. J. Bartoli, Experimental verification of the rainbow trapping effect in adiabatic plasmonic gratings, Proc. Natl. Acad. Sci. USA **108**, 5169 (2011).

[35] I. I. Smolyaninov, V. N. Smolyaninova, A. V. Kildishev, and V. M. Shalaev, Anisotropic Metamaterials Emulated by Tapered Waveguides: Application to Optical Cloaking, Phys. Rev. Lett. **102**, 213901 (2009).

[36] S. He, Y. He, and Y. Jin, Revealing the truth about 'trapped rainbow' storage of light in metamaterials, Sci. Rep. **2**, 583 (2012).

[37] A. F. Page, Ph.D. thesis, Imperial College London, 2015.

[38] H. Lira, Z. Yu, S. Fan, and M. Lipson, Electrically Driven Nonreciprocity Induced by Interband Photonic Transition on a Silicon Chip, Phys. Rev. Lett. **109**, 033901 (2012).

[39] A. Bahabad, M. M. Murnane, and H. C. Kapteyn, Quasi-phase-matching of momentum and energy in nonlinear optical processes, Nat. Photonics **4**, 570 (2010).

[40] M. Castellanos Muñoz, A. Yu. Petrov, L. O'Faolain, J. Li, T. F. Krauss, and M. Eich, Optically Induced Indirect Photonic Transitions in a Slow Light Photonic Crystal Waveguide, Phys. Rev. Lett. **112**, 053904 (2014).

[41] Q. Xu, P. Dong, and M. Lipson, Breaking the delay-bandwidth limit in a photonic structure, Nat. Phys. **3**, 406 (2007).

[42] M. F. Yanik and S. Fan, Stopping Light All Optically, Phys. Rev. Lett. **92**, 083901 (2004).

[43] Z. Yu and S. Fan, Complete optical isolation created by indirect interband photonic transitions, Nat. Photonics **3**, 91 (2009).

[44] T. A. Weiss and Y. Sivan, Pulse propagation in the slow and stopped light regime, Opt. Express **26**, 19294 (2018).

[45] A. Yariv and P. Yeh, *Photonics*, 6th ed. (Oxford University Press, Oxford, England, 2007).

[46] Y. Sivan and J. B. Pendry, Broadband time-reversal of optical pulses using a switchable photonic-crystal mirror, Opt. Express **19**, 14502 (2011).

[47] A. Chumak, V. Tiberkevich, A. Karenowska, A. Serga, J. Gregg, A. Slavin, and B. Hillebrands, All-linear time-reversal by a dynamic artificial crystal, Nat. Commun. **1**, 141 (2010).

[48] J. R. Zurita-Sanchez, P. Halevi, and J. C Cervantes-Gonzalez, Reflection and transmission of a wave incident on a slab with time-periodic dielectric function $\epsilon(t)$, Phys. Rev. A **79**, 053821 (2009).

[49] J. R. Zurita-Sanchez, P. Halevi, and J. C Cervantes-Gonzalez, Resonances in the optical response of a slab with time-periodic dielectric function $\epsilon(t)$, Phys. Rev. A **81**, 053834 (2010).

[50] Y. Sivan and J. B. Pendry, Time Reversal in Dynamically Tuned Zero-Gap Periodic Systems, Phys. Rev. Lett. **106**, 193902 (2011).

[51] Y. Sivan and J. B. Pendry, Theory of wave-front reversal of short pulses in dynamically tuned zero-gap periodic systems, Phys. Rev. A **84**, 033822 (2011).

[52] S. Hagness and A. Taflove, *Computational Electrodynamics: The Finite-Difference Time-Domain Method*, 3rd ed. (Artech House, Boston, MA, 2000).

[53] B. Dana, L. Lobachinsky, and A. Bahabad, Spatio-temporal coupled-mode theory in dispersive media under a dynamic modulation, Opt. Commun. **324**, 165 (2014).

[54] S. Lavdas and N. C. Panoiu, Theory of pulsed four-wave mixing in one-dimensional silicon photonic crystal slab waveguides, Phys. Rev. B **93**, 115435 (2016).

[55] Y. Sivan, S. Rozenberg, and A. Halstuch, Coupled-mode theory for electromagnetic pulse propagation in dispersive media undergoing a spatiotemporal perturbation: Exact derivation,

numerical validation, and peculiar wave mixing, Phys. Rev. B **93**, 144303 (2016).

[56] P. Lalanne, W. Yan, K. Vynck, C. Sauvan, and J.-P. Hugonin, Light interaction with photonic and plasmonic resonances, Laser Photonics Rev. **12**, 1700113 (2018).

[57] P. Y. Chen, D. J. Bergman, and Y. Sivan, Generalizing Normal Mode Expansion of Electromagnetic Green's Tensor to Lossy Resonators in Open Systems, Phys. Rev. Appl. **11**, 044018 (2019).

[58] T. Weiss, Pulse dynamics in the stopped and slow light regime, Ph.D. thesis, Ben-Gurion University, http://www.bgu.ac.il/~sivanyon/, 2019.

[59] G. P. Agrawal, *Nonlinear Fiber Optics* (Academic Press, San Diego, CA, 2011).

[60] Y. Sivan, S. Rozenberg, A. Halstuch, and A. Ishaaya, Nonlinear wave mixing of short pulses of different spatio-temporal extents, Sci. Rep. **6**, 29010 (2015).

[61] R. W. Boyd, *Nonlinear Optics*, 3rd ed. (Academic Press, Boston, MA, 2008).

[62] C. M. de Sterke and J. E. Sipe, Envelope-function approach for the electrodynamics of nonlinear periodic structures, Phys. Rev. A **38**, 5149 (1988).

[63] C. M. de Sterke, K. R. Jackson, and B. D. Robert, Nonlinear coupled-mode equations on a finite interval: A numerical procedure, J. Opt. Soc. Am. B **8**, 403 (1991).

[64] C. M. de Sterke, D. G. Salinas, and J. E. Sipe, Coupled-mode theory for light propagation through deep nonlinear gratings, Phys. Rev. E **54**, 1969 (1996).

[65] C. M. de Sterke and J. E. Sipe, in *Progress in Optics XXXIV*, edited by E. Wolf (North-Holland, Amsterdam, 1994), p. 203.

[66] F. Masia, W. Langbein, and P. Borri, Measurement of the dynamics of plasmons inside individual gold nanoparticles using a femtosecond phase-resolved microscope, Phys. Rev. B **85**, 235403 (2012).

[67] A. Shamir, A. Halstuch, Y. Sivan, and A. Ishaaya, Ns-duration transient Bragg gratings in silica fibers, Opt. Lett. **42**, 4748 (2017).

[68] R. W. Boyd, *Nonlinear Optics*, 2nd ed. (Academic Press, New York, 2003).

[69] M. Lipson, Guiding, modulating, and emitting light on silicon – Challenges and opportunities, J. Lightwave Technol. **23**, 4222 (2005).

[70] T. G. Euser, Ultrafast optical switching of photonic crystals, Ph.D. thesis, University of Twente, 2007.

[71] Y. Sivan and M. Spector, Ultrafast dynamics of optically-induced heat gratings in metals – More complicated than expected, arXiv:1909.03122.

[72] Y. Sivan, G. Ctistis, E. Yüce, and A. P. Mosk, Femtosecond-scale switching based on excited free-carriers, Opt. Express, **23**, 16416, 2015.

[73] A. R. Katko, S. Gu, J. P. Barrett, B.-I. Popa, G. Shvets, and S. A. Cummer, Phase Conjugation and Negative Refraction using Nonlinear Active Metamaterials, Phys. Rev. Lett. **105**, 123905 (2010).

[74] E. Galiffi, P. Arroyo-Huidobro, and J. B. Pendry, Broadband Nonreciprocal THz Amplification in Tuminal Graphene Metasurfaces, Phys. Rev. Lett. **123**, 206101 (2019).

[75] W. Li, B. Chen, C. Meng, W. Fang, Y. Xiao, X. Li, Z. Hu, Y. Xu, L. Tong, H. Wang, W. Liu, J. Bao, and Y. Ron Shen, Ultrafast all-optical graphene modulator, Nano letters **14**, 955 (2014).

[76] V. Bacot, M. Labousse, A. Eddi, M. Fink, and E. Fort, Revisiting time reversal and holography with spacetime transformations, Nat. Phys. **12**, 972 (2016).

[77] G. G. Rozenman, S. Fu, A. Arie, and L. Shemer, Quantum mechanical and optical analogies in surface gravity water waves, Fluids **4**, 96 (2019).